Research Square

Preprints are preliminary reports that have not undergone peer review.
They should not be considered conclusive, used to inform clinical practice,
or referenced by the media as validated information.

LINC01419/miR-132-3p/USP38 Axis Mediates High Glucose-Induced Ferroptosis in Vascular Endothelial Cells

Keke Tang
The First Affiliated Hospital of Ningbo University, Ningbo University
Wenjie Gao
The First Affiliated Hospital of Ningbo University, Ningbo University
Xinxin Wo
The First Affiliated Hospital of Ningbo University, Ningbo University
Zhouhong Mao
The First Affiliated Hospital of Ningbo University, Ningbo University
Hainan Ye
137582869330163.com

Tongde Hospital of Zhejiang Provincial

Article

Keywords: LINC01419, miR-132-3p, USP38, ferroptosis, vascular endothelial cells, T2DM

Posted Date: June 23rd, 2026

DOI: https://doi.org/10.21203/rs.3.rs-9970883/v1

License: This work is licensed under a Creative Commons Attribution 4.0 International License.
Read Full License

Additional Declarations: No competing interests reported.

Version of Record: A version of this preprint was published at Scientific Reports on August 31st, 2026.
See the published version at https://doi.org/10.1038/s41598-026-67890-3.

Abstract

Long non-coding RNA LINC01419 has been implicated in ferroptosis in various pathological conditions, yet its role in type 2 diabetes mellitus (T2DM) associated vascular endothelial dysfunction remains unclear. This study investigated the mechanism by which LINC01419 modulates ferroptosis in human vascular endothelial cells under high-glucose conditions. A high-glucose cellular model was established to evaluate cell proliferation, ferroptosis, and oxidative stress. Bioinformatics predictions and dual-luciferase reporter assays confirmed direct interactions between LINC01419 and miR-132-3p, and between miR-132-3p and ubiquitin-specific peptidase 38 (USP38). Quantitative real-time PCR validated regulatory interactions within the LINC01419/miR-132-3p/USP38 axis. Cell viability, reactive oxygen species levels, and ferroptosis markers were assessed via CCK-8, ROS detection, and Western blotting. Results showed that high glucose upregulated LINC01419 and USP38, downregulated miR-132-3p, elevated ROS, suppressed proliferation, and induced ferroptosis, as evidenced by increased ACSL4 and COX2 and decreased FTH1 and GPX4. LINC01419 acted as a competing endogenous RNA for miR-132-3p, and both molecules oppositely regulated USP38 expression. Notably, USP38 knockdown reversed high-glucose-induced abnormalities, restoring proliferation and ferroptosis-related protein expression. These findings reveal that the LINC01419/miR-132-3p/USP38 axis mediates ferroptosis in vascular endothelial cells under hyperglycemia, and suggest USP38 as a potential therapeutic target for T2DM.

1 Introduction

Diabetes mellitus (DM) is a chronic metabolic disorder characterized by persistent hyperglycemia, which leads to a spectrum of vascular complications, including diabetic cardiomyopathy, retinopathy, and impaired wound healing. Endothelial dysfunction is a central pathological event in these complications, and recent evidence highlights ferroptosis as a key mechanism underlying hyperglycemia-induced endothelial injury[1–4].

Ferroptosis, driven by iron overload and lipid peroxidation, is suppressed by glutathione peroxidase 4 (GPX4)[5–6]. In diabetic contexts, hyperglycemia promotes endothelial ferroptosis through pathways involving iron dysregulation and reactive oxygen species accumulation[1,5,7]. Although therapeutic strategies targeting ferroptosis have shown promise in restoring endothelial function in diabetic models[8,9], the precise molecular regulators connecting hyperglycemia to endothelial ferroptosis remain incompletely understood.

Long non-coding RNAs (lncRNAs) have emerged as key modulators of ferroptosis. Notably, LINC01419 has been implicated in ferroptosis in other pathological settings[10–12], and a recent study reported that a high-glucose environment induces LINC01419 upregulation, driving metabolic reprogramming that promotes hepatocellular carcinoma cell growth[13]. This finding directly links LINC01419 to glucose metabolism and suggests its potential involvement in hyperglycemia-related pathologies; however, its specific role in mediating ferroptosis within diabetic endothelial cells has not been unexplored.

In this study, we investigate the involvement of LINC01419 in high glucose-induced vascular endothelial damage. We focus on elucidating its effects on endothelial cell proliferation, ferroptosis, and oxidative stress using gene manipulation approaches. Our aim is to identify novel molecular targets for treating diabetic vascular complications.

2 Material and Methods2.1 Reagents

TRIzol reagent (Sigma, Cat. No. T9424-100m), HiScript II Q RT SuperMix for qPCR (+ gDNA wiper) (Vazyme, Cat. No. R123-01), AceQ qPCR SYBR Green Master Mix (Vazyme, Cat. No. Q111-02), PCR primers (R&F type, Genewiz), CCK-8 kit (Sigma, Cat. No. 96992), fetal bovine serum (FBS; Cat. No. VS500T), Dulbecco's modified Eagle medium (DMEM, Corning, Cat. No. 10-013-CVR), pancreatin (Shanghai Chemical Reagent Company, Cat. No. T4665); apoptosis detection kit (eBioscience, Cat. No. 88-8007), BCA protein assay kit (HyClone-Pierce, Cat. No. 23225), pre-stained protein marker (Thermo Fisher Scientific, Cat. No. 26615/26617), Immobilon Western Chemiluminescent HRP Substrate (Millipore, Cat. No. RPN2232), GeneRuler 1 kb DNA Ladder (Thermo Scientific, Cat. No. #SM0311), NormalRunTM 250 bp-II DNA Ladder(GeneRay, Cat. No. #DL2502), PrimeSTAR HS DNA Polymerase (Takara, Cat. No. R010B), ClonExpress II One Step Cloning Kit (Vazyme, Cat. No. C122); EndoFree Midi Plasmid Kit (TIANGEN, Cat. No. #DP118-2); ampicillin sodium salt (Genebase, Cat. No. A100339-0025); reactive oxygen species (ROS) detection kit (Solarbio, Cat. No. CA1420); colorimetric iron assay kit (abcam, Cat. No. ab83366).

2.2 Equipment

The following equipment was used: a Nanodrop spectrophotometer (Thermo Fisher Scientific, Model 2000/2000C), vertical electrophoresis system (Shanghai Tianneng), real-time PCR instrument (ABI, Model VII7), flow cytometer (Millipore, Guava easyCyte HT), fluorescence microscope (Olympus, Model IX71), centrifuge (Lu Xiangyi, Model TDZ5-WS), chemiluminescence imaging system (GE Healthcare, Model AI600), Bluepard constant-temperature incubator (Shanghai Yiheng Scientific Instrument Co., Ltd., Model GHP-9080), and high-speed centrifuge (Thermo Scientific, Model Legend Micro 17).

2.3 Prediction of downstream targets of LINC01419

Interactions between lncRNAs and microRNAs are mainly mediated by complementary base pairing. To identify potential downstream targets of LINC01419, we predicted lncRNA-miRNA interactions using the specialized bioinformatics database starBase. This analysis revealed that the LINC01419 sequence contained multiple sites complementary to the seed region of miR-132-3p. Subsequently, to explore the downstream effects, we identified USP38 as a key predicted target of miR-132-3p using the TargetScan database.

2.4 Cell culture

Human vascular endothelial cells (HUVECs, Procell, Cat# CP-H082) were cultured in two different media for 48 h: conventional medium(D-Glucose:5.5mmol/L) and high-glucose medium (D-

Glucose:30.5mmol/L). For transfection experiments, HUVECs were transfected with a synthesized LINC01419 overexpression plasmid and miR-132-3p mimics and then divided into three groups: (1) LINC01419 control group + miRNA control group, (2) LINC01419 overexpression group + miRNA control group, and (3) LINC01419 overexpression group + miRNA mimics group.

2.5 Dual-Luciferase Reporter Assay

To verify whether miR-132-3p directly targets the USP38 3'UTR, a dual-luciferase reporter assay was performed. Wild-type (WT) and mutant (MUT) reporter plasmids (psiCHECK-2-USP38-3'UTR-WT/MUT) were constructed by cloning synthetic DNA into the psiCHECK-2 vector. 293T cells were co-transfected with these plasmids and either miR-132-3p mimics or control mimics. After 48 h, Renilla luciferase activity was measured using the Dual-Luciferase Reporter Assay System (Promega) and normalized to firefly luciferase activity. Each assay was performed in triplicate, with three independent biological replicates.

2.6 CCK-8 assay

HUVECs were seeded in 96-well plates (3×10^3 cells/well) in 100 μL EGM-2. At 24, 48, 72, 96, and 120 h post-seeding, 10 μL CCK-8 reagent was added and incubated at 37°C for 2 h. Absorbance was measured at 450 nm (reference 630 nm) using a microplate reader.

2.7 Western blot analysis

Total proteins were extracted with RIPA buffer and quantified by BCA assay. Equal amounts (20 μg/lane) were separated by 10% SDS-PAGE and transferred to PVDF membranes. After blocking with 5% non-fat milk in TBST (1 h, RT), membranes were incubated overnight at 4°C with primary antibodies: anti-FTH1 (1:2000, abcam, ab75972), anti-COX-2 (1:2000, abcam, ab179800), anti-GPX4 (1:2000, abcam, ab125066), anti-ACSL4 (1:5000, abcam, ab155282), and anti-GAPDH (1:3000, Affinity, AF7021) as loading control. After TBST washes, membranes were incubated with HRP-conjugated goat anti-rabbit secondary antibody (1:3000, Affinity, S0001) for 1 h at RT. Protein bands were visualized using ECL substrate on a Tanon imaging system.

2.8 Quantitative real-time PCR assay

Total RNA was extracted from transfected HUVECs using TRIzol, and its concentration was determined by Nanodrop spectrophotometry (Thermo 2000/2000C). RNA (1 μg) was reverse-transcribed into cDNA per the manufacturer's protocol. qRT-PCR was performed on an IQ5 cycler with SYBR Green Master Mix in 8 μL reactions containing 5 μL 2× SYBR Green mix, 0.25 μL each primer (10 μM), 2 μL cDNA, and 2.3 μL nuclease-free water. Cycling conditions: 95°C for 30 s, then 40 cycles of 95°C for 5 s and 60°C for 30 s. Melting curve analysis verified primer specificity. All reactions were run in triplicate. Target gene expression was normalized to U6 and calculated using the $2^{(-\Delta\Delta Ct)}$ method. Primer sequences are listed in Table 1.

2.9 Detection of intracellular reactive oxygen species (ROS)

Intracellular ROS were detected using dihydroethidium (DHE). HUVECs were seeded in 96-well plates (1×10^5 cells/well) and incubated with 200 μL DHE staining solution (10 μM) in the dark at 37°C for 30 min. All subsequent steps were performed under minimal light to avoid photobleaching. After washing twice with 1×PBS, red fluorescence (excitation 510–560 nm, emission 590–620 nm) was observed.

2.10 Detection of intracellular iron level

Intracellular iron levels were measured using a colorimetric iron assay kit (Solarbio) following the manufacturer's instructions. The reaction wells were prepared as follows: 5 ul of iron reducer was added to each standard well. For the measurement of Fe^{2+}, 5 μl of kit's assay buffer from the kit was added to each sample well. To determine total iron (Fe^{2+} + Fe^{3+}), 5 μl of iron reducer was added to each sample well. After thorough mixing, all the standard and sample wells were incubated at 37°C for 30 min. Subsequently, 100 μl of iron detection reagent was added to each well, and the plates were incubated in the dark at 37°C for 60 min. The absorbance at 593 nm was immediately measured using a microplate spectrophotometer. Iron concentrations were calculated based on the standard curve.

2.11 Statistical analysis

All statistical analyses were preformed using SPSS software (version 19.0; SPSS, Inc., Chicago, IL, USA). Quantitative data are presented as the mean ± standard deviation from at least three independent experiments. Between-group comparisons were analyzed using the Student's t-test, with statistical significance defined as $^{**}P < 0.01$, and $^{***}P < 0.001$.

3 Results

3.1 High glucose activates ferroptosis in HUVECs

To assess the effect of high glucose levels on ferroptosis, we conducted in vitro experiments to evaluate the cellular phenotypic changes. CCK-8 assays revealed that HUVEC proliferation in the high-glucose (HG) group was significantly reduced compared with the normal control (NC) group ($P < 0.001$; Fig. 1A). DCFH-DA staining showed significantly higher ROS levels in the HG group than in the NC group (Fig. 1B). Western blot confirmed upregulated ferroptosis markers (ACSL4, COX2) and downregulated regulatory proteins (FTH1, GPX4) in the HG group (Fig. 1C). These results demonstrate that high-glucose conditions not only inhibit HUVEC proliferation and exacerbate oxidative stress but also activate ferroptosis, highlighting its critical role in HG-induced vascular endothelial injury.

3.2 Effect of high glucose on expression of LINC01419, miR-132-3p, and USP38

qRT-PCR analysis revealed that high glucose significantly upregulated LINC01419 and downregulated miR-132-3p (both $P < 0.001$, Fig. 2A-B). Consistently, Western blot showed markedly increased USP38 expression in the HG group ($P < 0.001$, Fig. 2C). These findings indicate that high glucose enhances LINC01419 and USP38 expression while suppressing miR-132-3p.

3.3 Validation of the LINC01419/miR-132-3p/USP38 reuglatory axis

3.3.1 LINC01419 directly binds to miR-132-3p

Dual-luciferase assays were performed in 293T cells co-transfected with miR-132-3p mimics and either the wild-type (LINC01419-wt) or mutated (LINC01419-mut) reporter plasmids. Compared with the negative control (cells co-transfected with miR-132-3p mimics and empty vector), luminescence signals were significantly reduced in cells transfected with LINC01419-wt, whereas no significant change was observed in cells with LINC01419-mut (Fig. 3A). These results confirm a direct and specific binding between LINC01419 and miR-132-3p via the predicted sites.

3.3.2 LINC01419 acts as a ceRNA for miR-132-3p

To validate the ceRNA mechanism between LINC01419 and miR-132-3p, we examined their reciprocal regulatory relationship. qPCR analysis revealed that overexpression of LINC01419 significantly downregulated miR-132-3p expression, whereas transfection with the miR-132-3p mimic significantly reduced LINC01419 expression (Fig. 3B). Furthermore, rescue experiments demonstrated that co-transfection of the LINC01419 overexpression plasmid with the miR-132-3p mimic reversed these individual effects: LINC01419 expression was attenuated, while miR-132-3p expression was restored (Fig. 3B). Together, these data confirm the mutually inhibitory relationship and establish LINC01419 as a ceRNA that sponges miR-132-3p.

3.3.3 miR-132-3p directly targets USP38

Dual-luciferase assays were performed in 293T cells co-transfected with miR-132-3p mimics and a wild-type USP38 3'-UTR reporter (USP38-3'UTR-WT). Luciferase activity was significantly reduced versus the empty-vector control, but remained unchanged when the binding sites were mutated (USP38-3'UTR-MUT) (Fig. 3C), confirming that miR-132-3p directly targets the USP38 3'-UTR and represses its expression.

3.3.4 LINC01419 and miR-132-3p oppositely regulate USP38

To further validate the regulatory relationships among LINC01419, miR-132-3p, and USP38, we overexpressed LINC01419 or miR-132-3p in 293T cells and measured USP38 mRNA levels by qRT-PCR. Compared with the negative control (NC) group (cells transfected with empty vector), the relative expression of USP38 was significantly upregulated in the LINC01419-OE group ($P < 0.001$, Fig. 3D). In

contrast, USP38 expression was significantly downregulated in the miR-132-3p mimic group relative to the NC group ($P < 0.001$, Fig. 3E). These opposite effects are consistent with the ceRNA mechanism, where LINC01419 sponges miR-132-3p to release USP38 from post-transcriptional repression.

3.4 The effects of the LINC01419/miR-132-3p/USP38 axis on cellular functions

3.4.1 LINC01419 and miR-132-3p regulate ferroptosis of HUVECs under high-glucose conditions

CCK-8 results showed that overexpression of LINC01419 significantly inhibited the proliferation of HUVECs, while overexpression of miR-132-3p significantly promoted it. Additionally, miR-132-3p overexpression partially reversed the inhibitory effect of LINC01419 on cell proliferation (Fig. 4A). Western blot results showed that overexpression of LINC01419 promoted ferroptosis in HUVECs by upregulating ACSL4 and COX2 and downregulating FTH1 and GPX4. In contrast, overexpression of miR-132-3p inhibited ferroptosis and partially reversed the pro-ferroptotic effect (Fig. 4B). Intracellular iron ion detection results indicated that overexpression of LINC01419 significantly increased iron accumulation, while overexpression of miR-132-3p significantly reduced it, and the latter partially reversed the pro-accumulation effect of the former (Fig. 4C). ROS detection results showed that overexpression of LINC01419 significantly increased ROS levels in HUVECs, promoting oxidative stress; whereas overexpression of miR-132-3p significantly reduced ROS levels, inhibiting oxidative stress, and partially reversed the pro-oxidative stress effect of LINC01419 (Fig. 4D).

3.4.2 USP38 knockdown reverses high glucose-induced ferroptosis in HUVECs

To investigate the role of USP38 in HG-induced HUVEC injury, we constructed USP38-knockdown lentiviruses (shUSP38) and transduced them into HUVECs. After exposure to HG levels, we systematically evaluated USP38 protein expression and cell function. Compared with the NC group, the USP38 protein level was significantly increased in the HG group. In contrast, the USP38-knockdown + high glucose (shUSP38 + HG) group showed a significant decrease in USP38 protein expression compared with the HG group(Fig. 2C). qPCR results showed that miR-132-3p levels were significantly lower in the HG group than in the NC group. However, miR-132-3p levels were significantly restored in the shUSP38 + HG group compared with the HG group (Fig. 5A). CCK-8 proliferation assays showed that at 48 h post-treatment, cells exposed to HG levels had significantly reduced proliferation compared with normal controls. Notably, USP38 knockdown significantly enhanced proliferative capacity under hyperglycemic conditions. From day 3, the shUSP38 + HG group showed significantly higher proliferation rates than the HG group (Fig. 5B). Western blot analysis revealed that, compared with the NC group, the HG group had significantly downregulated FTH1 and GPX4 expression, accompanied by significantly upregulated ACSL4 levels. In the shUSP38 group, FTH1 expression remained unchanged, whereas GPX4

was significantly upregulated, and ACSL4 was significantly downregulated. Additionally, the shUSP38 + HG group had significantly higher FTH1 and GPX4 expression but significantly lower ACSL4 levels than the HG group (Fig. 5C). ROS detection assays showed that ROS levels were significantly higher in the HG group than in the NC group, whereas the shUSP38 group had significantly lower ROS levels. Importantly, the shUSP38 + HG group showed significantly lower ROS levels than the HG group (Fig. 5D).

4 Discussion

Chronic hyperglycemia-induced endothelial dysfunction is a pivotal trigger for diabetic macrovascular complications, involving oxidative stress, inflammation, and advanced glycation end-product (AGE) accumulation [14–17]. In the present study, we demonstrated that high glucose (HG) inhibits proliferation and induces ferroptosis in HUVECs, as evidenced by the upregulation of ACSL4 and COX2, downregulation of FTH1 and GPX4, increased intracellular iron accumulation, and elevated ROS levels. These observations align with the established role of ferroptosis in diabetic endothelial injury [18–22] and confirm that ferroptosis and oxidative stress are mutually reinforcing in this context.

Mechanistically, we identified the LINC01419/miR-132-3p/USP38 axis as a novel signaling cascade mediating HG-induced endothelial ferroptosis. HG significantly upregulated LINC01419 and USP38 while downregulating miR-132-3p. Bioinformatics analysis combined with dual-luciferase reporter assays confirmed that LINC01419 directly targets miR-132-3p [23,24], and qRT-PCR further revealed a reciprocal negative regulation between LINC01419 and miR-132-3p. Functional experiments showed that LINC01419 overexpression mimicked the detrimental effects of HG, whereas miR-132-3p overexpression exerted protective effects and partially reversed LINC01419-induced damage. These findings are consistent with the known protective role of miR-132-3p in endothelial cells through pathways involving RASA1/RAS/PI3K/AKT and EndMT regulation [25,26].

Importantly, we identified USP38 as a downstream target of miR-132-3p. Dual-luciferase reporter assays demonstrated direct binding of miR-132-3p to the 3'UTR of USP38, and overexpression of miR-132-3p significantly suppressed USP38 expression. Conversely, USP38 knockdown upregulated miR-132-3p, suggesting a bidirectional regulatory relationship. USP38, a deubiquitinase of the ubiquitin-specific protease family, has been implicated in various malignancies [27–29], but its role in diabetic vascular complications remains largely unexplored. Our results showed that USP38 knockdown in HUVECs under HG conditions significantly enhanced proliferation, reduced apoptosis, downregulated ACSL4, upregulated FTH1 and GPX4, and decreased ROS levels. These findings align with recent reports that USP38 promotes ferroptosis in diabetic cardiomyopathy and atrial fibrillation models by stabilizing IRP2 and interacting with ACAD11, leading to iron overload and lipid peroxidation [30,31].

Collectively, our study establishes a working model in which HG upregulates LINC01419, which acts as a ceRNA to sponge miR-132-3p, thereby relieving its suppression of USP38. Elevated USP38 then promotes ferroptosis through iron metabolism dysregulation and lipid peroxidation, ultimately contributing to endothelial dysfunction. This is the first report to demonstrate the involvement of the

LINC01419/miR-132-3p/USP38 axis in HG-induced endothelial ferroptosis, providing a previously unrecognized molecular basis for diabetic macrovascular complications.

Several limitations of the present study must be noted. First, all findings are based on in vitro experiments using HUVECs; in vivo validation using diabetic animal models is needed. Second, the expression levels of LINC01419, miR-132-3p, and USP38 in vascular tissues from diabetic patients and their correlation with clinical vascular function indices require confirmation. Third, although we demonstrated the regulatory role of USP38 in ferroptosis, whether USP38 directly deubiquitinates key ferroptosis regulators such as GPX4, ACSL4, or IRP2 remains to be determined.

In summary, our study identifies the LINC01419/miR-132-3p/USP38 axis as a key mediator of HG-induced endothelial ferroptosis and dysfunction, providing novel insights into diabetic macrovascular disease pathogenesis and potential therapeutic targets.

5 Conclusions

High-glucose conditions upregulate LINC01419 and downregulate miR-132-3p, collectively impairing HUVEC proliferation and promoting ferroptosis. Mechanistically, LINC01419 functions as a ceRNA that sequesters miR-132-3p, thereby disrupting the miR-132-3p/USP38 axis and driving ferroptosis in vascular endothelial cells under T2DM conditions. Importantly, USP38 knockdown reversed HG-induced proliferation suppression, ferroptosis promotion, and oxidative damage, identifying USP38 as a key mediator of glucotoxic endothelial injury.

Declarations

Acknowledgments

We thank all participants, as well as the members of the Endocrinology Department (The First Affiliated Hospital of Ningbo University) and the Clinical Lab (Tongde Hospital of Zhejiang Provincial), for their cooperation and support.

Author Contributions

K.T. wrote the main manuscript text.

X.W. carried out the experiments and prepared the figures.

W.G. performed data curation.

Z.M. contributed to methodology.

H.Y. supervised the study and reviewed & edited the manuscript.

All authors reviewed the manuscript.

Ethics Approval and Consent to Participate

This study was approved by the Medical Ethics Committee of the First Affiliated Hospital of Ningbo University (approval number: KY 20220902) and was performed in accordance with the ethical standards of the Declaration of Helsinki. Written informed consent was obtained from all individual participants included in the study.

Data Availability Statement

The datasets used or analyzed during the current study are available from the corresponding author on reasonable request.

Funding

This work was supported by the Zhejiang Provincial Medical and Health Research Project (grant number 2025HY0953).

Competing interests

The authors declare no competing interests.

References

1. Luo, C. et al. Hyperglycemia-induced DNA damage response activates DNA-PK complex to promote endothelial ferroptosis in type 2 diabetic cardiomyopathy. *Theranostics* **15** (10), 4507–4525 (2025).
2. Chen, L. et al. CD74 ablation rescues type 2 diabetes mellitus-induced cardiac remodeling and contractile dysfunction through pyroptosis-evoked regulation of ferroptosis. *Pharmacol. Res.* **176**, 106086 (2022).
3. Tang, W. et al. Caveolin-1 alleviates diabetes-associated cognitive dysfunction through modulating neuronal ferroptosis-mediated mitochondrial homeostasis. *Antioxid. Redox Signal.* **37** (13–15), 867–886 (2022).
4. Ye, H. et al. Bioinformatics analysis identifies potential ferroptosis key gene in type 2 diabetic islet dysfunction. *Front. Endocrinol. (Lausanne)*. **13**, 904312 (2022).
5. Li, S. Y. et al. Ferroptosis in the ageing retina: A malevolent fire of diabetic retinopathy. *Ageing Res. Rev.* **93**, 102142 (2024).
6. Latunde-Dada, G. O. Ferroptosis: role of lipid peroxidation, iron and ferritinophagy. *Biochim. Biophys. Acta Gen. Subj.* **1861** (8), 1893–1900 (2017).
7. Jin, C. et al. A multifunctional hydrogel promotes diabetic wound healing by remodeling iron balance and energy metabolism. *Biomaterials* **326**, 12360 (2026).
8. Dong, Q. R. et al. Theory-screened Prussian blue analogues-based nanozymes for promoting diabetic wound healing via ferroptosis inhibition. *Mater. Today Bio*. **32**, 101839 (2025).

9. Lu, W. et al. Mesenchymal stem cell-derived extracellular vesicles accelerate diabetic wound healing by inhibiting NET-induced ferroptosis of endothelial cells. *Int. J. Biol. Sci.* **20** (9), 3515–3529 (2024).
10. Chen, J. L. et al. Overexpression of long noncoding RNA LINC01419 in esophageal squamous cell carcinoma and its relation to the sensitivity to 5-fluorouracil by mediating GSTP1 methylation. *Ther. Adv. Med. Oncol.* **11**, 1758835919838958 (2019).
11. Hou, Y. et al. LINC01419-mediated epigenetic silencing of ZIC1 promotes metastasis in hepatocellular carcinoma through the PI3K/Akt signaling pathway. *Lab. Invest.* **101** (5), 570–587 (2021).
12. Gu, Z., Wu, S., Wang, J. & Zhao, S. Long non-coding RNA LINC01419 mediates miR-519a-3p/PDRG1 axis to promote cell progression in osteosarcoma. *Cancer Cell. Int.* **20**, 147 (2020).
13. Liu, Y. et al. Effects of lncRNA LINC01419 targeting miR-320a on proliferation, migration and invasion of synovial fibroblasts in juvenile rheumatoid arthritis. *Chin. J. Immunol.* **38**, 414–418 (2022).
14. Khaddaj Mallat, R. et al. The vascular endothelium: A regulator of arterial tone and interface for the immune system. *Crit. Rev. Clin. Lab. Sci.* **54** (7–8), 458–470 (2017).
15. Chen, M. et al. Gingerenone A attenuates diabetic vascular remodeling through AMPK/mTOR/S6K1 signaling. *Front. Pharmacol.* **17**, 1706103 (2026).
16. Am, C. Endothelial response to glucose: dysfunction, metabolism, and transport. *Biochem. Soc. Trans.* **49** (1), 313–325 (2021).
17. Cao, J. et al. Peroxidasin promotes diabetic vascular endothelial dysfunction induced by advanced glycation end products via NOX2/HOCl/Akt/eNOS pathway. *Redox Biol.* **45**, 102031 (2021).
18. Gawargi, F. I. & Mishra, P. K. Regulation of cardiac ferroptosis in diabetic human heart failure: uncovering molecular pathways and key targets. *Cell. Death Discov*. **10** (1), 268 (2024).
19. Malaviya, P., Kumar, J. & Kowluru, R. A. Role of ferroptosis in mitochondrial damage in diabetic retinopathy. *Free Radic Biol. Med.* **225**, 821–832 (2024).
20. Song, J. et al. Licochalcone D mitigates intracerebral hemorrhage-induced ferroptosis of neurons through COX2 inhibition. *Front. Pharmacol.* **16**, 1566724 (2025).
21. Kang, P. et al. Argon Alleviates Bone Cancer Pain by Mitigating Neuronal Ferroptosis via the TLR2-COX-2 Pathway. *Front. Biosci. (Landmark Ed)*. **30** (9), 43761 (2025).
22. Li, C. et al. Mechanistic studies on the regulation of ferroptosis by ferritin 1 through the FTH1 signaling pathway affecting oocyte maturation. *Theriogenology* **249**, 117658 (2026).
23. Sun, Z. P., Tan, Z. G. & Peng, C. Long noncoding RNA LINC01419 promotes hepatocellular carcinoma malignancy by mediating miR-485-5p/LSM4 axis. *Kaohsiung J. Med. Sci.* **38** (9), 826–838 (2022).
24. Gu, Z. et al. Long non-coding RNA LINC01419 mediates miR-519a-3p/PDRG1 axis to promote cell progression in osteosarcoma. *Cancer Cell. Int.* **20**, 147 (2020).
25. Hulshoff, M. S. et al. miR-132-3p and KLF7 as novel regulators of aortic stiffening-associated EndMT in type 2 diabetes mellitus. *Diabetol. Metab. Syndr.* **15** (1), 11 (2023).

26. Li, S. et al. Artificial mesenchymal stem cell extracellular vesicles enhanced ischemic stroke treatment through targeted remodeling brain microvascular endothelial cells. *Acta Pharm. Sin B*. **15** (8), 4248–4264 (2025).
27. Zhang, T. et al. Ubiquitin specific peptidase 38 epigenetically regulates KLF transcription factor 5 to augment malignant progression of lung adenocarcinoma. *Oncogene* **43** (16), 1190–1202 (2024).
28. Zhao, S. et al. USP38 functions as an oncoprotein by downregulating the p53 pathway through deubiquitination and stabilization of MDM2. *Cell Death Differ.* **32** (6), 1128–1141 (2025).
29. Wang, J. et al. USP38 inhibits colorectal cancer cell proliferation and migration via downregulating HMX3 ubiquitylation. *Cell. Cycle*. **22** (10), 1169–1181 (2023).
30. Xiao, Z. et al. Ubiquitin-specific protease 38 promotes atrial fibrillation in diabetic mice by stabilizing iron regulatory protein 2. *Free Radic Biol. Med.* **224**, 88–102 (2024).
31. Xiao, Z. et al. Ubiquitin-specific protease 38 exacerbates diabetic cardiomyopathy via post-translational modification of ACAD11. *Redox Biol.* **84**, 103704 (2025).

Table

Table 1 is not available with this version.

Figures

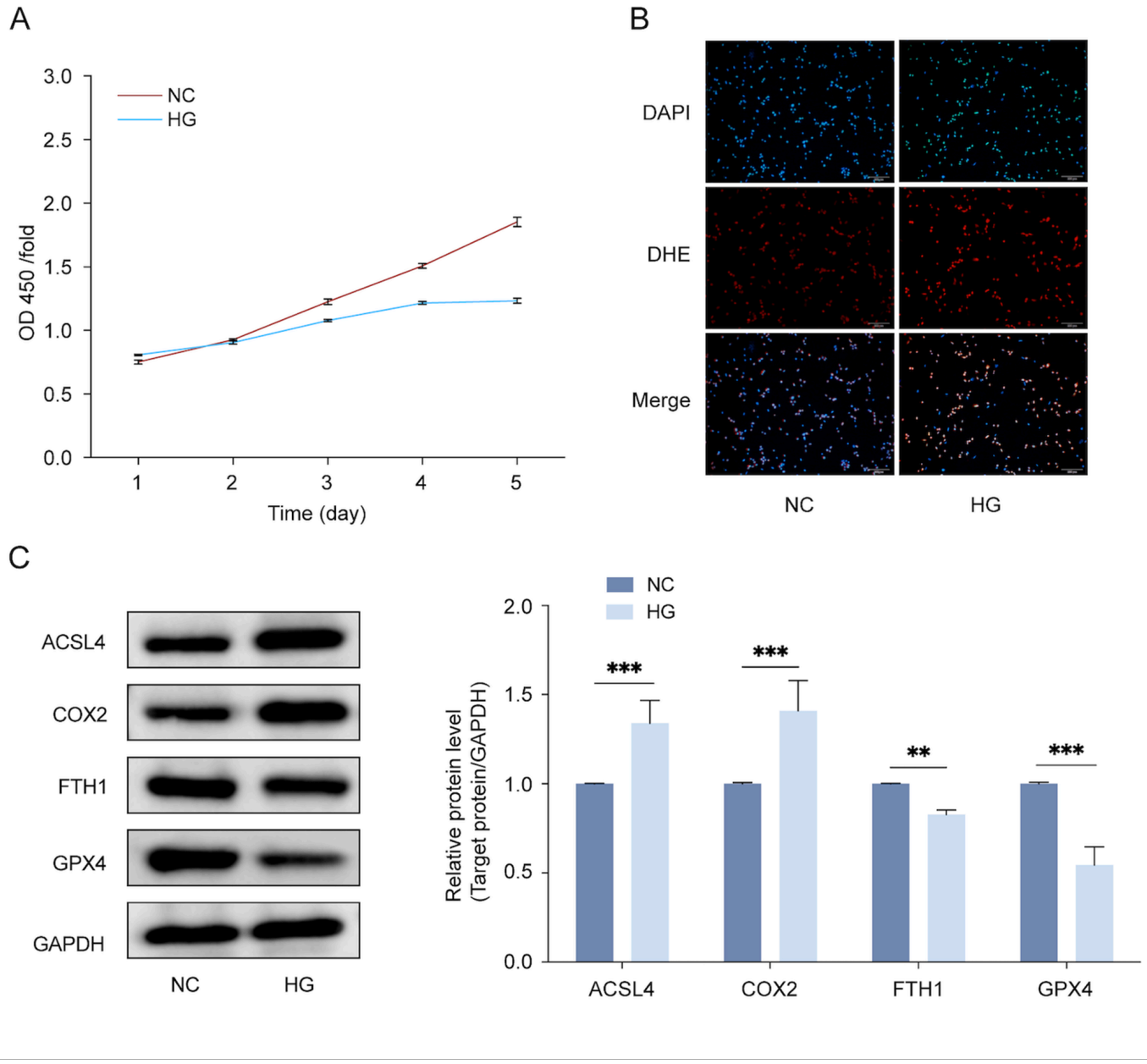


Figure 1

Effects of high glucose on ferroptosis. (A) CCK-8 assay showedreduced HUVEC proliferation under high glucose. (B) ROS detection indicated increased reactive oxygen species levels in HG-treated cells. (C) Western blot analysis revealed upregulation of ACSL4 and COX2,and downregulation of FTH1 and GPX4 in the HG group.

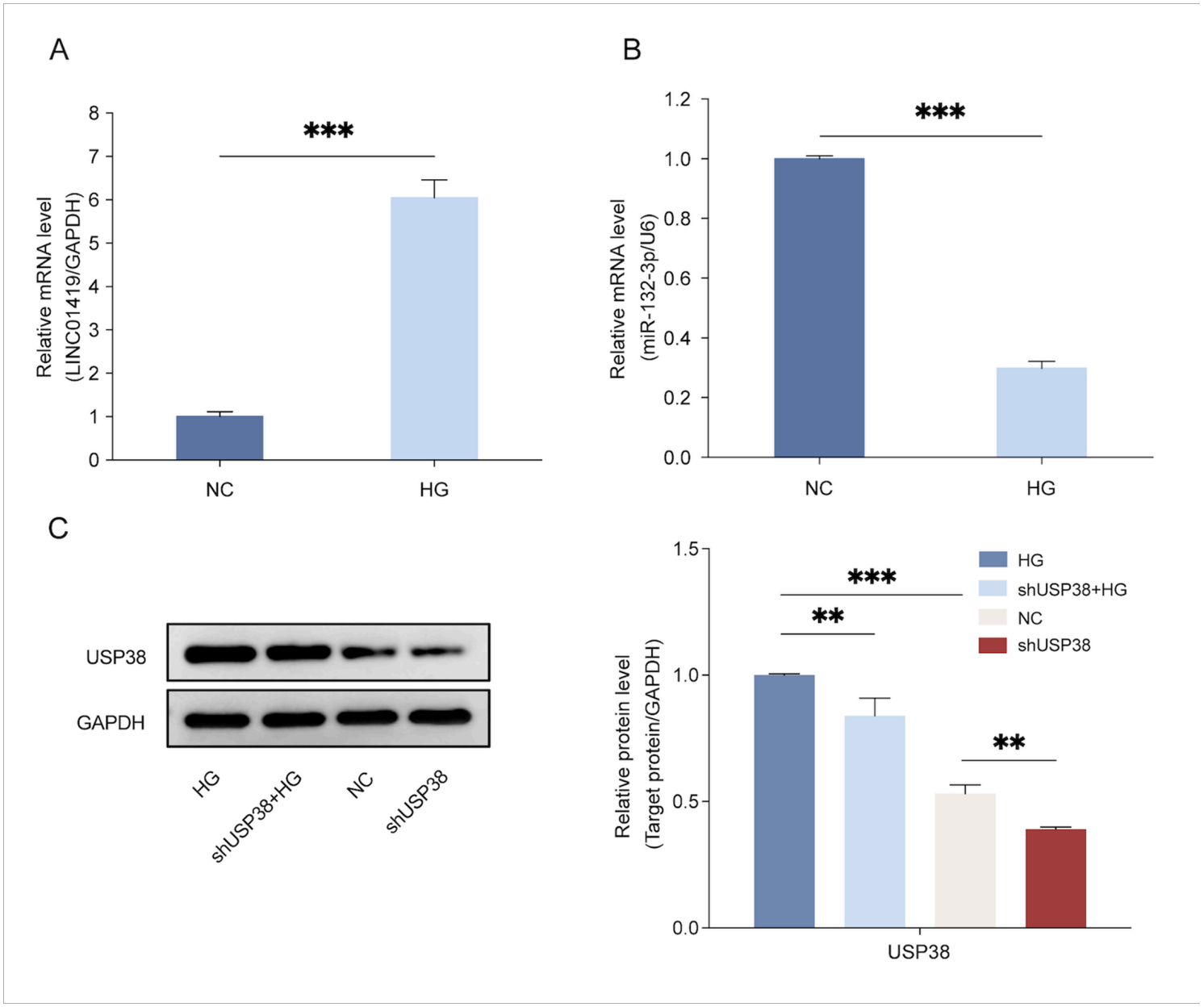


Figure 2

Effect of high glucose on expression of LINC01419, miR-132-3p, and USP38. (A) qRT-PCR results showed increased LINC01419 expression in the HG group. (B) qRT-PCR results showed decreased miR-132-3p expression in the HG group. (C) Western blot analysis revealed increased USP38 expression in the HG group compared with the NC group.

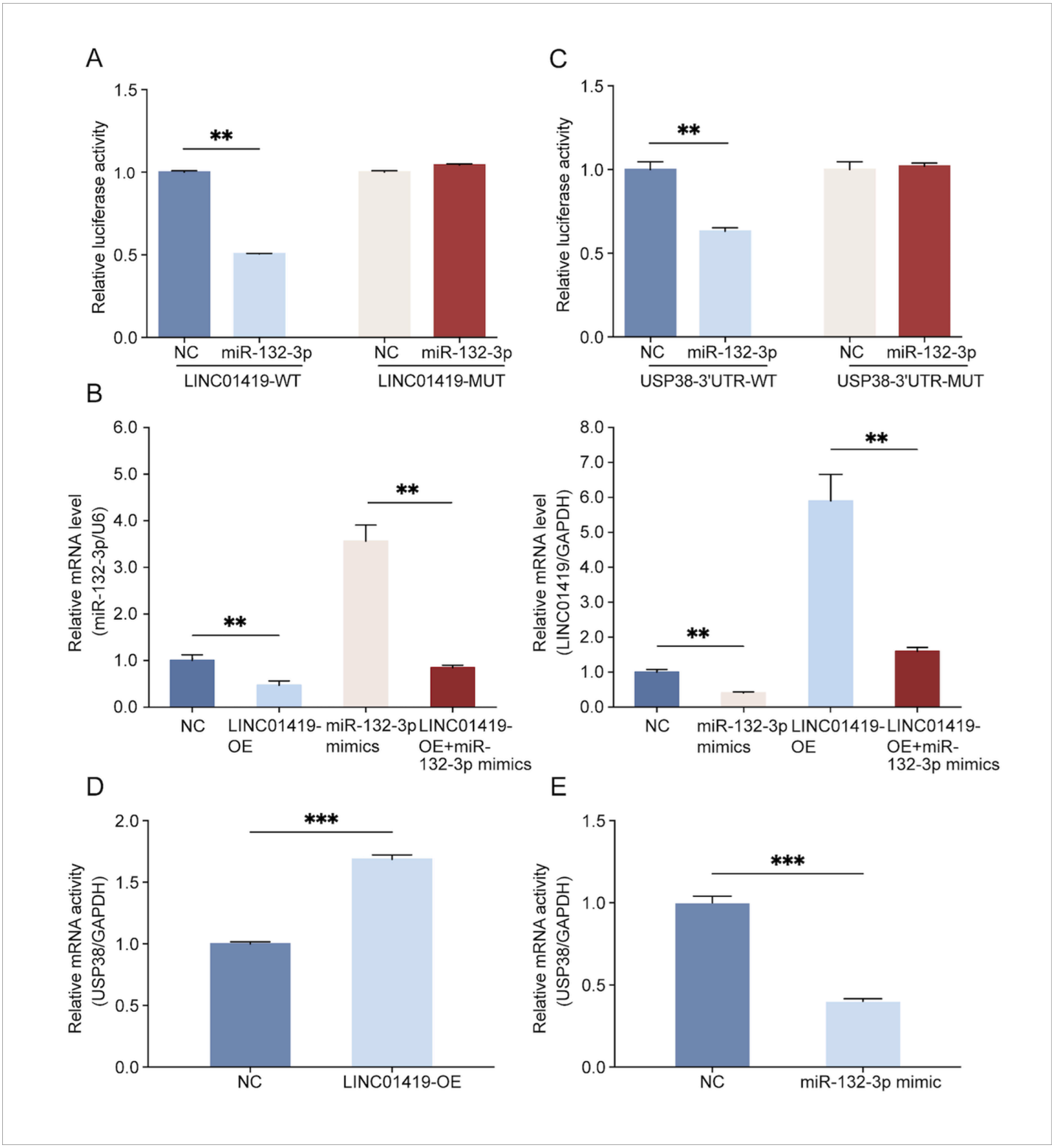


Figure 3

LINC01419 and miR-132-3p oppositely regulate USP38 expression (A) Dual-luciferase reporter assay (with co-transfection of miR-132-3p mimics) validates the direct binding between LINC01419 and miR-132-3p. (B) qRT-PCR analysis demonstrates the reciprocal ceRNA relationship: LINC01419 overexpression downregulates miR-132-3p, whereas miR-132-3p mimic transfection reduces LINC01419 expression.(C) Dual-luciferase reporter assay (with co-transfection of miR-132-3p mimics) confirms that

miR-132-3p directly targets the 3'-UTR of USP38. (D) qRT-PCR shows that LINC01419 overexpression upregulates USP38 mRNA.(E) Conversely, miR-132-3p mimic transfection downregulates USP38 expression compared with the NC group.

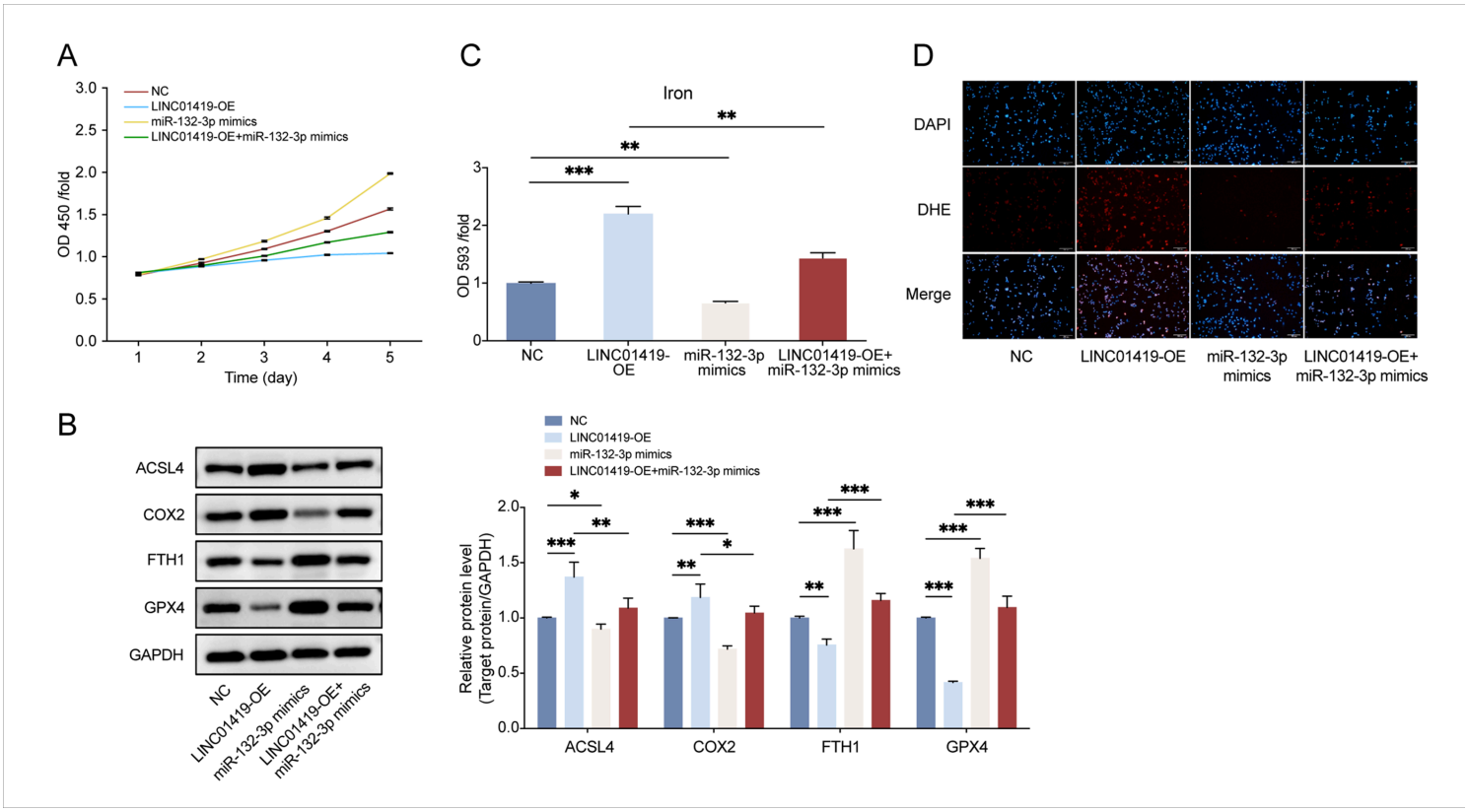


Figure 4

LINC01419 and miR-132-3p regulate ferroptosis in HUVECs under high-glucose conditions. (A) Cell proliferation detected by CCK-8 assay. (B) Western blot analysis of ACSL4, COX2, FTH1, and GPX4 protein expression. (C) Intracellular iron content. (D) Intracellular ROS levels.

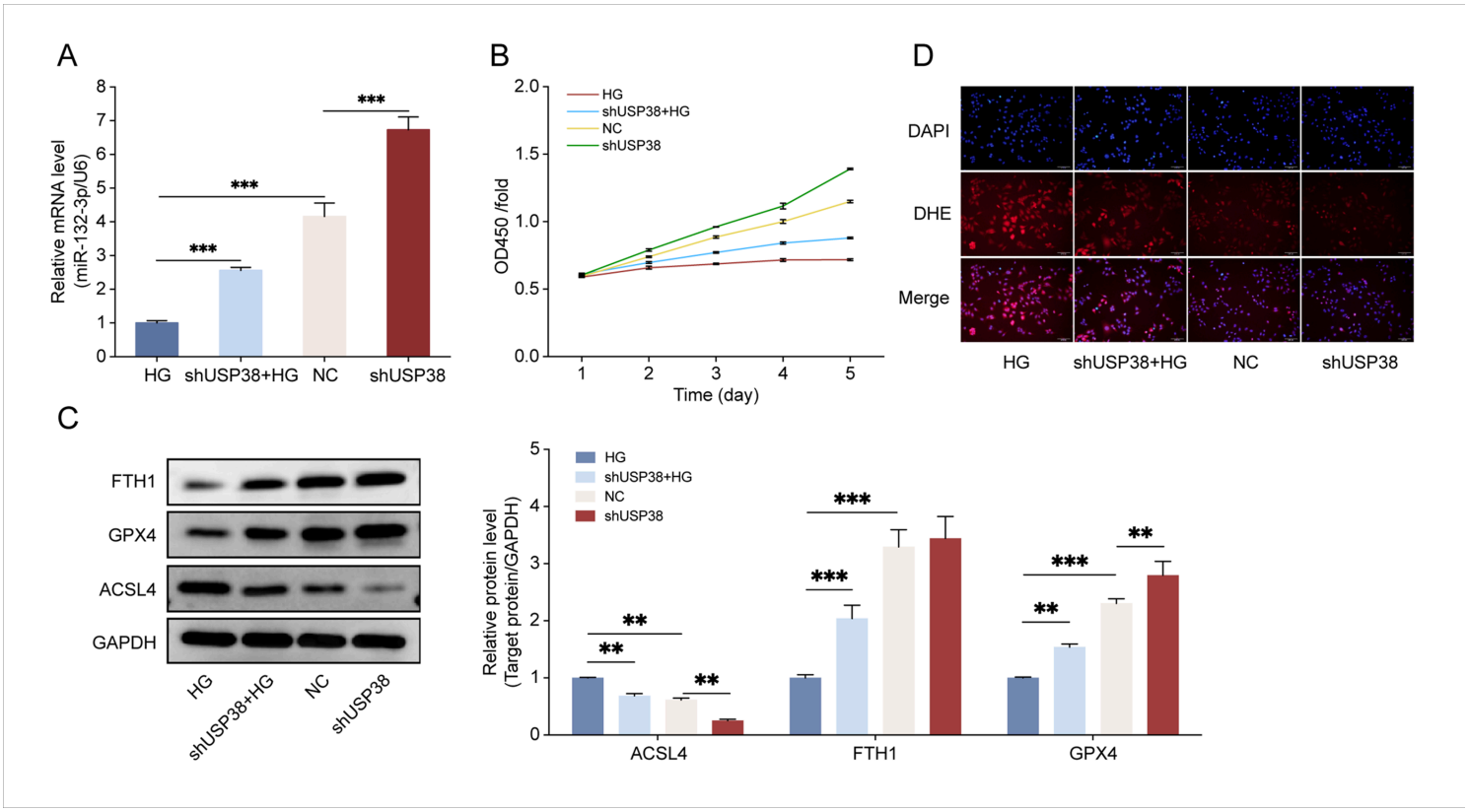


Figure 5

USP38 knockdown reverses high glucose-induced ferroptosis in HUVECs. (A) Relative expression levels of miR-132-3p detected by qPCR. (B) Cell proliferation assessed by CCK-8 assay. (C) Protein expression levels of FTH1, GPX4, and ACSL4 analyzed by Western blot. (D) Intracellular ROS levels.

Supplementary Files

This is a list of supplementary files associated with this preprint. Click to download.

- figureWBmark.pdf